Applied Physics Letters

RESEARCH ARTICLE | APRIL 13 2026

Digitally programmable kirigami metamaterials via magnetic encoding

Qinlian Kang ; Jinbo Yang ; Chenyang Ji ; Zhijun Lin ; Songyu Xiong; Yongfeng Mei ; Jizhai Cui

Appl. Phys. Lett. 128, 151902 (2026)
https://doi.org/10.1063/5.0318941

AIP Publishing

Applied Physics Letters ARTICLE pubs.aip.org/aip/apl

Digitally programmable kirigami metamaterials via magnetic encoding

Cite as: Appl. Phys. Lett. **128**, 151902 (2026); doi: 10.1063/5.0318941
Submitted: 22 December 2025 · Accepted: 25 March 2026 ·
Published Online: 13 April 2026

View Online Export Citation CrossMark

Qinlian Kang,[1,2,3] Jinbo Yang,[1,2,3] Chenyang Ji,[1,2,3] Zhijun Lin,[1,2,3] Songyu Xiong,[1,2,3] Yongfeng Mei,[1,2,3] and Jizhai Cui[1,2,3,a)]

AFFILIATIONS

[1]State Key Laboratory of Surface Physics and International Institute for Intelligent Nanorobots and Nanosystems, College of Intelligent Robotics and Advanced Manufacturing, Fudan University, Shanghai 200438, China
[2]Shanghai Key Laboratory of Metasurfaces for Light Manipulation, Fudan University, Shanghai 200433, China
[3]Zhejiang Key Laboratory of Extreme Environment Functional Materials, Yiwu Research Institute of Fudan University, Yiwu 322000, Zhejiang, China

[a)]Author to whom correspondence should be addressed: jzcui@fudan.edu.cn

ABSTRACT

The vast configuration space of magnetic metamaterials, enabled by embedding reversibly orientable magnets into rotating-square kirigami pixels, remains largely unexplored beyond uniform magnetization patterns. To navigate this space, in-plane magnetic orientations are treated as binary bits, creating $2^{N\times N}$ possible states for an $N \times N$ lattice. A Monte Carlo approach, combined with a mapping of all configurations onto an N^2-dimensional hypercube, allows for the systematic statistical enumeration of energy landscapes and single-bit reconfiguration paths. This framework classifies stability into neutral, monostable, bistable, and tristable classes, with occurrence probabilities converging to approximately 0, 0.6013, 0.3981, and 0.0006 as system size increases. Programmable responses—including tension–compression asymmetric stiffness, snap-through instability, and a two-stage absorption/locking energy dissipation mode—are demonstrated. The resulting digital, graph-based platform points to applications in soft modular robotics, impact-mitigation layers, deployable structures, and mechanical logic.

Mechanical metamaterials derive their unusual responses from architecture.[1–3] By periodically arranging functional structural units ("pixels") into lattice assemblies, they realize counterintuitive behaviors, such as auxeticity,[4,5] negative stiffness,[6–8] and programmable shape reconfigurations.[9–11] Reconfigurable mechanical metamaterials embed stimuli-responsive mechanisms that modulate either the intrinsic properties of individual pixels or their spatial organization, enabling on-demand tuning of macroscopic mechanics for diverse applications.[12–17] Recent studies further leverage pixel-level multistability to switch among discrete stable states and thereby tailor global stress–strain responses, stiffness, and functional responses.[18–23]

Among them, magnetic interactions provide a long-range, orientation-dependent coupling mechanism,[24] enriching material responses, such as mechanical wave transmission,[25–28] multistablility,[27] locomotion,[29] and information processing.[30,31] Leveraging this, recent magneto-kirigami platforms embed permanent magnets into rotating-square (RS) kirigami lattices, showing that tuning magnet orientations enables substantial reprogrammability of static and dynamic responses.[32] Additionally, the nonlinear, orientation-dependent dipole–dipole interactions can be switched between repulsive and attractive by controlling neighboring orientations, driving reversible phase transitions.[33] In the RS kirigami, tensile actuation simultaneously alters inter-panel spacing and relative orientation, thereby reshaping the magnetic potential energy and the ensuing mechanical behavior. These magnetic mechanical metamaterials offer the advantage of reprogrammability. However, previous work has largely been confined to uniform magnetization patterns, lacking a systematic method to explore the vast configuration space and tunability afforded by non-uniform patterns.

Here, we present a systematic, statistical exploration of the configuration space for magnetic RS kirigami lattices, employing a hypercube representation and Monte Carlo-style sampling to predict and classify their mechanical responses. In this framework, the magnetic orientation of each pixel is treated as a binary state. For an $N \times N$ metamaterial, this results in $2^{N\times N}$ orientation configurations, each yielding a distinct nonlinear energy–displacement response. This enables programmable transitions among neutrally stable (flat energy landscape with respect to the kirigami opening angle), monostable, bistable, and

tristable behaviors. To navigate this vast design space, we introduce a compact orientation encoding and map all configurations onto the vertices of an $N \times N$-dimensional hypercube, where traversing an edge corresponds to flipping a single pixel's magnetic orientation. Over this graph, we construct a stability landscape (defined by the number and location of energy minima), which reveals connectivity and families of reconfiguration pathways that allow controlled changes in the count and positions of stable states. Leveraging the diversity of energy landscapes across configurations, this approach can further demonstrate selective control of global stiffness and energy absorption. Taken together, the binary encoding and hypercube mapping establish a digital, graph-based framework for planning reconfigurations and for the inverse design of target stiffness and dissipation profiles. Moving beyond binary encoding toward multi-level magnetization and spatially graded dipole strength would unlock a combinatorially richer set of responses; furthermore, the hypercube formalism provides a principled basis for algorithmic path search when integrated with field-programmable orientation-addressing schemes. Beyond numerical analysis, integrating finite element analysis with machine learning can enhance simulation accuracy and efficiency while enabling the reversible design of functional properties.[34–37]

Inspired by the RS mechanism of kirigami, we envision a class of reprogrammable mechanical metamaterials whose structural configuration can be reconfigured *in situ* to meet application-specific requirements. The RS lattice consists of rigid square panels connected at their vertices by ideal hinges of negligible stiffness and zero friction, so that geometry dominates and the role of magnet orientation can be isolated [Fig. 1(a)]. Let l_0 denote the side length of a square and θ as the half-opening angle, defined as the in-plane rotation of each square about its hinge; neighboring squares rotate by $\pm\theta$. With θ from 0° to 90°, the center-to-center spacing l between adjacent panels first increases and then decreases, accompanied by alternating rotations of neighboring squares,

$$l = \sqrt{2} l_0 \sin(\theta + 45^\circ), \tag{1}$$

$$\theta_i = (-1)^i \theta. \tag{2}$$

In this system, a positive rotation ($\theta > 0^\circ$) is defined as clockwise (CW), and a negative rotation ($\theta < 0^\circ$) as counterclockwise (CCW). To magnetically couple otherwise kinematically connected pixels, we embed permanent magnets into the panels. When modeling magnetic interactions in elastic metamaterials, typical methods include finite element analysis,[34,36,37] a Morse potential for out-of-plane moments,[25,26] and a dipole model for in-plane moments.[28,33] In our study, the embedded hard magnets exhibit in-plane orientation, and we aim to explore a configuration space encompassing $2^{N\times N}$ possible configurations. Considering both computational efficiency and physical fidelity, we adopt the magnetic dipole model (further details on the model's

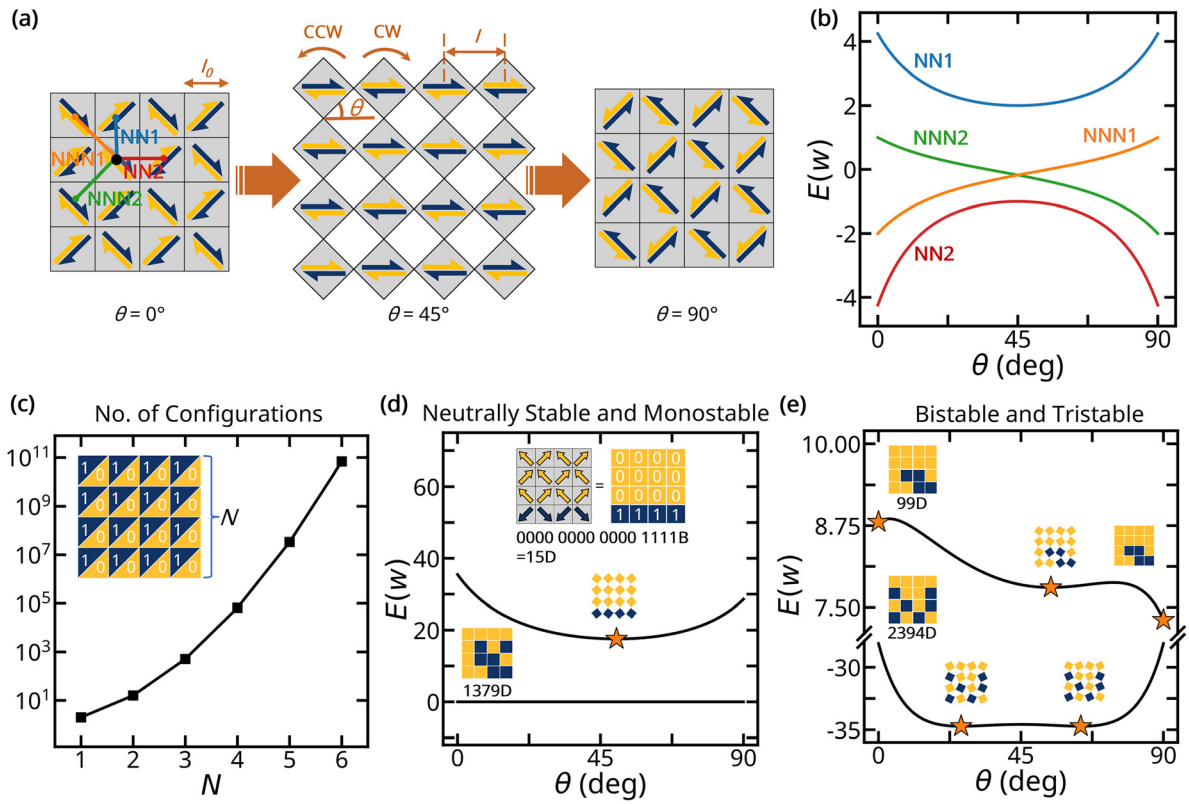

FIG. 1. Design concepts. (a) RS kirigami lattice with embedded permanent magnets. (b) Dipole–dipole interaction energies $E(\theta)$ for representative NN and NNN magnet pairs, demonstrating long-range, orientation-dependent magnetic coupling. (c) Exponential growth of the configuration space with system size N. (d)–(e) Examples of the four stability classes (neutral, mono-, bi-, and tristable) for an $N = 4$ system, with corresponding configuration codes and stable states (yellow stars).

applicability in supplementary material Sec. VII). The pairwise dipole–dipole interaction energy between magnetic moments $\mathbf{m}_i$ and $\mathbf{m}_j$ at positions $\mathbf{r}_i$ and $\mathbf{r}_j$ is[38]

$$E_{ij} = \frac{\mu_0}{4\pi {r_{ij}}^3}\left[\mathbf{m}_i \cdot \mathbf{m}_j - 3\left(\mathbf{m}_i \cdot \hat{\mathbf{r}}_{ij}\right)\left(\mathbf{m}_j \cdot \hat{\mathbf{r}}_{ij}\right)\right], \tag{3}$$

where $\mathbf{r}_{ij} = \mathbf{r}_i - \mathbf{r}_j$, $r_{ij} = |\mathbf{r}_{ij}|$, $\hat{\mathbf{r}}_{ij} = \mathbf{r}_{ij}/r_{ij}$. The total magnetic energy of the whole system is[38]

$$E_{\text{total}} = \sum\nolimits_{i<j}^{N^2} E_{ij}. \tag{4}$$

The distance r_{ij} is a function of θ. This geometric dependence directly modifies the total energy calculation (supplementary material Sec. II). Because tensile actuation changes both inter-panel distances and relative magnet orientations [Eqs. (1) and (2)], the magnetic potential E_{ij} nonlinearly depends on θ, thereby shaping the total magnetic potential E_{total} of the system [Fig. 1(b)]. In this paper, the energy normalization factor is defined as $w = \mu_0 m^2/4\pi\left(\sqrt{2}l_0\right)^3$. Consequently, flipping the orientation of a single magnet can globally reconfigure the energy landscape and the resulting macroscopic mechanical response (Fig. S1 in the supplementary material).

To enumerate and control the exponentially many magnetization patterns, we adopt a binary orientation encoding. Each panel carries one magnet whose in-plane orientation is treated as a binary digit, with "0" assigned to the upper-left or upper-right diagonal and "1" to the lower-left or lower-right diagonal at $\theta = 0°$. Reading an $N \times N$ array in row-major order yields an N^2-bit sequence that uniquely labels a configuration, enabling systematic exploration of a vast configuration space of size $2^{N\times N}$ [Fig. 1(c)]. For simplicity, we use the decimal equivalent of this binary string [e.g., the binary configuration code "0000 0000 0000 1111B" is represented as a decimal code "15D" in Fig. 1(d)].

We analyze the energy landscape of the magneto-kirigami metamaterial by tracking how the total potential energy E_{total} evolves with the opening angle θ (see the derivation in the supplementary material). From the landscape, one can determine the number and locations of stable states, the energy barriers that must be overcome for transitions, and the associated force–displacement characteristics as well as effective stiffness.[39]

In a size $N = 4$ system, reorienting magnets reveals four stability classes. Neutrally stable, monostable, bistable, and tristable examples are shown in Figs. 1(d) and 1(e), together with the corresponding encoded configurations; yellow stars mark stable states. The four stabilities can be experimentally accessible with NdFeB (N52) magnets in a 3D-printed polylactic acid (PLA) matrix if the dipole-model error is <1.3%, which requires normalized spacings of $\sqrt{3}$ (cube side length), 1.46 (radial cylinder diameter), and 1.52 (axial cylinder diameter). The diameter-to-length ratio is $\sqrt{4/3}$ for cylinder magnets (see details in supplementary material Sec. VII). In the tristable case [Fig. 1(e)], minima occur near both end states (0° and 90°) and at an intermediate angle (≈54.45°), arising from geometric self-locking tendency at facet contact (end states) combined with attractive dipole–dipole interactions.[40]

We numerically determine the stability class for all configurations in a 4×4 RS system (Table I), finding monostable (58.40%) and bistable (41.29%) configurations dominate. System size influences stability:

TABLE I. Multistability probabilities. Values calculated in each case from every possible orientation distribution.

System size N	Neutrally stable	Monostable	Bistable	Tristable
2	0.5	0.25	0.25	0
3	0	0.5859	0.4063	0.0078
4	0.0015	0.5840	0.4129	0.0016
5	0	0.5909	0.4083	0.0008

Neutral stability is absent for $N = 3$ and $N = 5$, and the tristable proportion decreases with N. These observations suggest that neutral stability is associated with highly symmetric layouts and that the probability of the neutrally stable class diminishes with system size, approaching a steady distribution where monostable and bistable classes dominate (approximately 0.6 and 0.4, respectively). The exponential growth of configuration space (e.g., 2^{25} for $N = 5$) makes exhaustive enumeration infeasible for larger N. This motivates a Monte Carlo sampling (5×10^6 random configurations per system) for size $N > 5$. With increasing N, the probabilities converge to 0.6013 (monostable), 0.3981 (bistable), and 0.0006 (tristable), while neutrally stable probability remains zero (Fig. S4 in the supplementary material).

Figure 2 maps the configuration space of $N \times N$ RS kirigami lattices onto the vertices of an $N \times N$-dimensional hypercube.[41] Each vertex represents a binary orientation configuration and adjacent vertices differ by exactly one bit (a single-pixel flip), which corresponds to reorienting a single pixel. Coloring the vertices by the number of stable states in the associated energy landscape yields a visual summary of stability classes and their connectivity. This graph therefore serves as a quantitative guide for planning reconfiguration paths that traverse edges and alter mechanical behavior through single-pixel flips.

Hypercube networks for $N = 2$, 3, and 4 [Figs. 2(a)–2(c)] reveal that despite exponential growth in configuration space with N, vertices of the same stability class form distinct clusters. The color distribution mirrors the statistics reported for 4×4 arrays in Table I, dominated by monostable and bistable classes, with neutrally stable and tristable classes being rare.

The hypercube network supports diverse reconfiguration pathways for regulating both the number and the locations of stable states. Figures 2(d) and 2(e) show two representative reconfiguration paths for $N = 4$. One path [Fig. 2(d)] sequences through all four stability classes via single-bit flips, while another [Fig. 2(e)] maintains monostability but relocates the energy minimum. The corresponding energy-angle curves [Figs. 2(d-ii) and 2(e-ii)] confirm these behaviors. Besides open paths, closed loops (bit-flip cycles) in the hypercube are feasible, enabling cyclic regulation of stability properties; examples are shown in Figs. S5 and S6 in the supplementary material. These establish a digital, graph-based platform for planning reconfiguration sequences and for tailoring stiffness and energy absorption in metamaterials.

Further, by using this energy expression and the principle of virtual work, we obtain the quasi-static force–displacement relationship (the detailed derivation of the force–displacement relationship in the supplementary material Sec. II). The metamaterial exhibits distinct mechanical responses under tensile versus compressive load depending

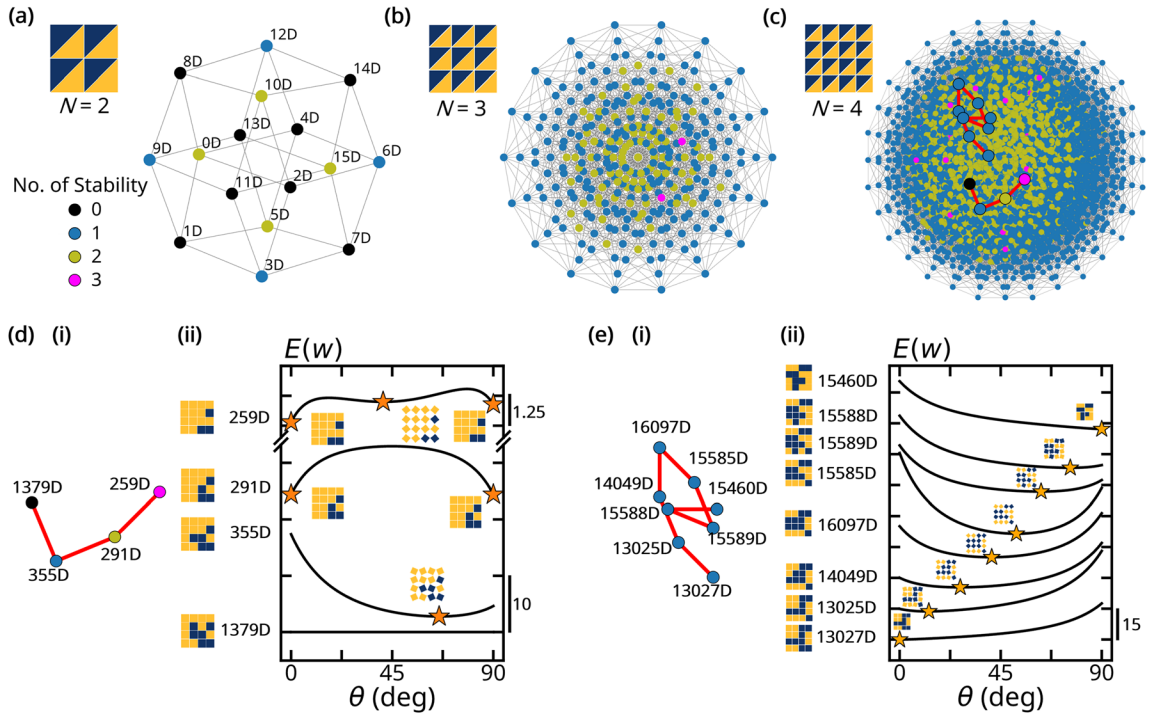

FIG. 2. Hypercubic representation and digital reprogrammability of stability configurations. (a)–(c) Hypercube stability graphs for $N = 2$ (a), $N = 3$ (b), and $N = 4$ (c). Vertices represent binary orientation configurations; edges connect configurations differing by a single-pixel (one-bit) flip. (d) and (e) Representative one-bit reconfiguration pathways showing continuous regulation of (d) the number of stable states and (e) the location of a stable state. Figures (d-i) and (e-i) are magnified views of the routes marked by red lines in (c). Panels (ii) show the corresponding energy-angle curves, with stars marking stable states.

on the encoded stable states (Fig. 3). The force–displacement curves in Figs. 3(a)–3(d) depict four representative behaviors. The system's path on these curves is selected by the initial stable state and the load direction (tension/compression) (detailed analysis in Sec. VI of the supplementary material).

Considering the case in which the stable state lies at an intermediate angle, namely $\theta \neq 0°$, $45°$, or $90°$. The metamaterial then supports bidirectional deformation and exhibits pronounced tension–compression asymmetry, as in Fig. 3(a). The tensile stiffness significantly exceeds the compressive stiffness, indicating higher structural compliance under compression. This tension–compression asymmetry originates from the differing kinematic efficiency of converting block rotation to macroscopic displacement on each loading branch (see the supplementary material for details). Selection between these branches is made by load reversal from its single stable state.

The metamaterial can exhibit snap-through instability, characterized by a rapid transition between two stable equilibrium states. Specifically, when the system resides in a stable state at end point [$\theta = 0°$ or $90°$, Fig. 3(b)], structural reconfiguration occurs only when the tensile force exceeds a critical value that overcomes the attractive dipole–dipole interactions responsible for the metastable state, because end point states are geometrically self-locked, requiring a finite force to overcome their energy barrier for switching. In Fig. 3(b), configuration 27D exhibits two independent snap-through events initiating from $\theta = 0°$ and $90°$ with different thresholds. Each path is accessed by starting from the corresponding end point state. Notably, a configuration stabilized at $\theta = 45°$ admits two distinct deformation branches under uniaxial compression, one with decreasing θ and the other with increasing θ (Fig. S7 in the supplementary material). Because the two branches have comparable stiffness, a bifurcation point emerges and the response becomes sensitive to small perturbations, which is useful for the design of mechanically assisted logic or switching elements.[42]

Beyond these basic behaviors, encoded magnetization can integrate multiple features, such as combining multiple asymmetric-stiffness levels [Fig. 3(c), configuration 1317D] or merging asymmetric stiffness with snap-through instability [Fig. 3(d), configuration 99D]. The desired response is selected by choosing the initial stable state or load direction. The richness of achievable responses stems from the multiple stabilities of the encoded landscape, enabling real-time functional adaptation without changing the encoding itself. Monotonic stiffness regulation is also achievable for structures sharing the same stable angle (Fig. S8 in the supplementary material).

We demonstrate that the digital mechanical metamaterial functions as a tunable and reusable energy absorber. Conventional absorbers rely on irreversible crushing or plastic deformation and therefore possess fixed, single-use properties.[43] In contrast, the present system achieves reprogrammability and recoverability through in-plane magnet reorientation, allowing the absorption profile to be reset or retargeted without replacing the structure.

Unlike conventional energy-absorbing materials, this system enables both multi-path energy capture and stable energy locking via two

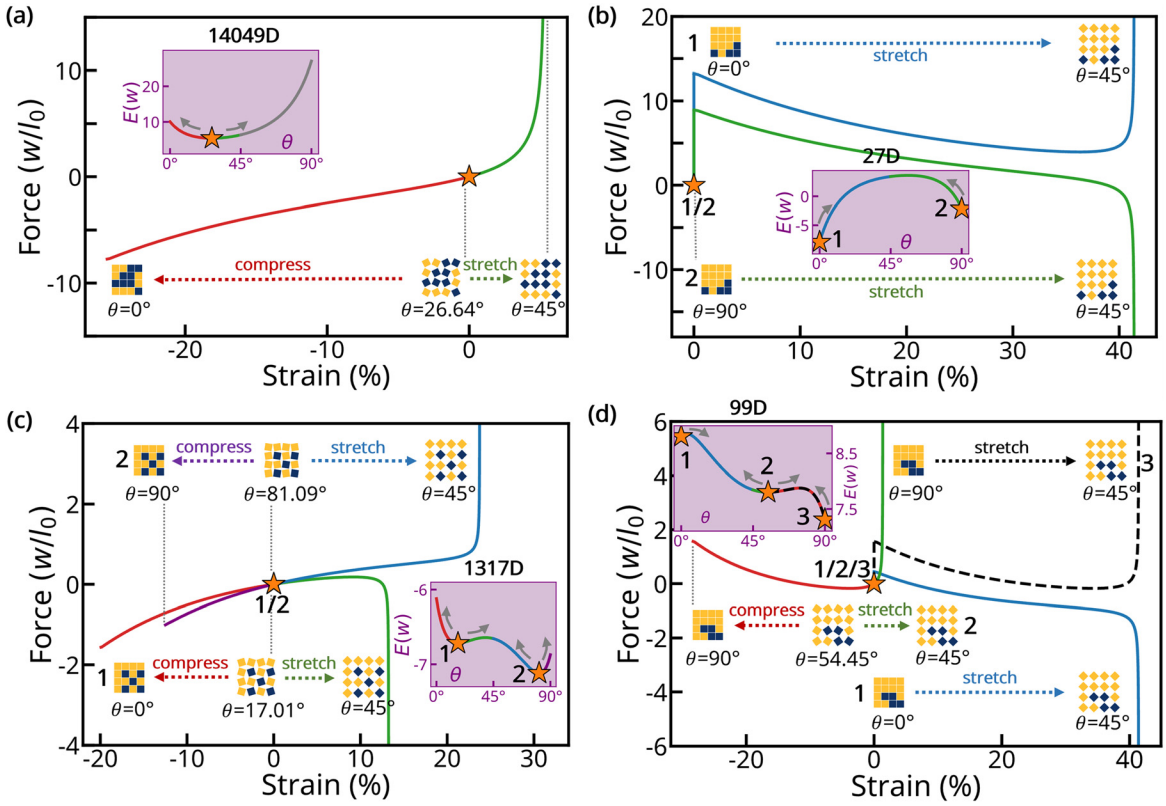

FIG. 3. Digitally reprogrammable stiffness. (a)–(d) Representative force–strain responses for four encoded configurations (codes above each panel). Strain is referenced to the starred stable state (negative/positive: compression/tension). Colored branches represent distinct deformation paths originating from the encoded stable states (stars). Path switching is achieved by either reversing the load direction from a given state or by selecting a different initial stable state (see the supplementary material Sec. VI for details). Discontinuous jumps indicating snap-through instability between stable states. Insets: total energy landscapes $E(\theta)$ vs opening angle θ; stars mark stable states. Colors match energy branches in insets to force–strain curves. For example, in (c), the red curves in both the main panel and the inset show the compression of the 1317D configuration starting from steady state 1.

complementary routes: compression and tension [Fig. 4(a)]. The process contains an initial absorption phase followed by an energy-locking phase. During absorption, the structure deforms under compression (e.g., from 29.3° to 0° for configuration 30D) or tension (to 45°), converting kinetic to magnetic potential energy and potentially reaching a high-energy unstable state. In the locking phase, a single magnet flip transitions the system from the unstable high-energy state to a nearby stable configuration [such as transitioning from configuration 30D to 22D by flipping the (4,1) magnet, or from 30D to 22D by flipping the (3,3) magnet], effectively locking in the stored energy. This may reduce the undesired rebound oscillations for energy absorbers, which is a key advantage in scenarios that require rapid dissipation without overshoot.

Figure 4(b) shows the energy absorption density vs strain for all $N = 4$ configurations (green curves), revealing a broadly tunable design space. The inset illustrates a single-flip reconfiguration path (e.g., 15 828D to 21 845D) that continuously modulates absorption capacity from $\sim 0.2 w/l_0^2$ to $\sim 3.9 w/l_0^2$ (highlighted orange curves). In Fig. 4(c), stripe-like orientation patterns (alternating horizontal or vertical bands, here horizontal band is shown) yield the highest energy absorption density, because nearest-neighbor dipoles across adjacent moments all experience attractive interactions (horizontal bands) or repulsive interactions (vertical bands), maximizing the net stored magnetic energy. Within the general framework, the maximum attainable absorption density increases with system size [Fig. 4(c)]. It rises from about $3.7\, w/l_0^2$ at $N = 2$ to about $5.4\, w/l_0^2$ at $N = 50$. Thus, absorber performance is size-dependent below a critical scale but converges to a limit thereafter.

In practical applications, performance depends on several factors (supplementary material Sec. VIII).[34,36,37] Substrate stiffness is critical: While a rigid substrate ensures magnets follow the intended deformation path, compliant materials would introduce complex, unpredictable magnet motions. Deformation speed also matters, as our quasi-static model does not account for inertial effects under rapid impact. Furthermore, strong magnetic interactions can induce physical and numerical instabilities, such as out-of-plane deformations, non-single-degree-of-freedom motions, or deviations from the ideal dipole model. Therefore, practical implementation requires ensuring material and design compatibility with the dipole model, or refining the model based on specific experimental parameters.

In summary, we present a reprogrammable mechanical metamaterial platform that integrates rotating-square kirigami with

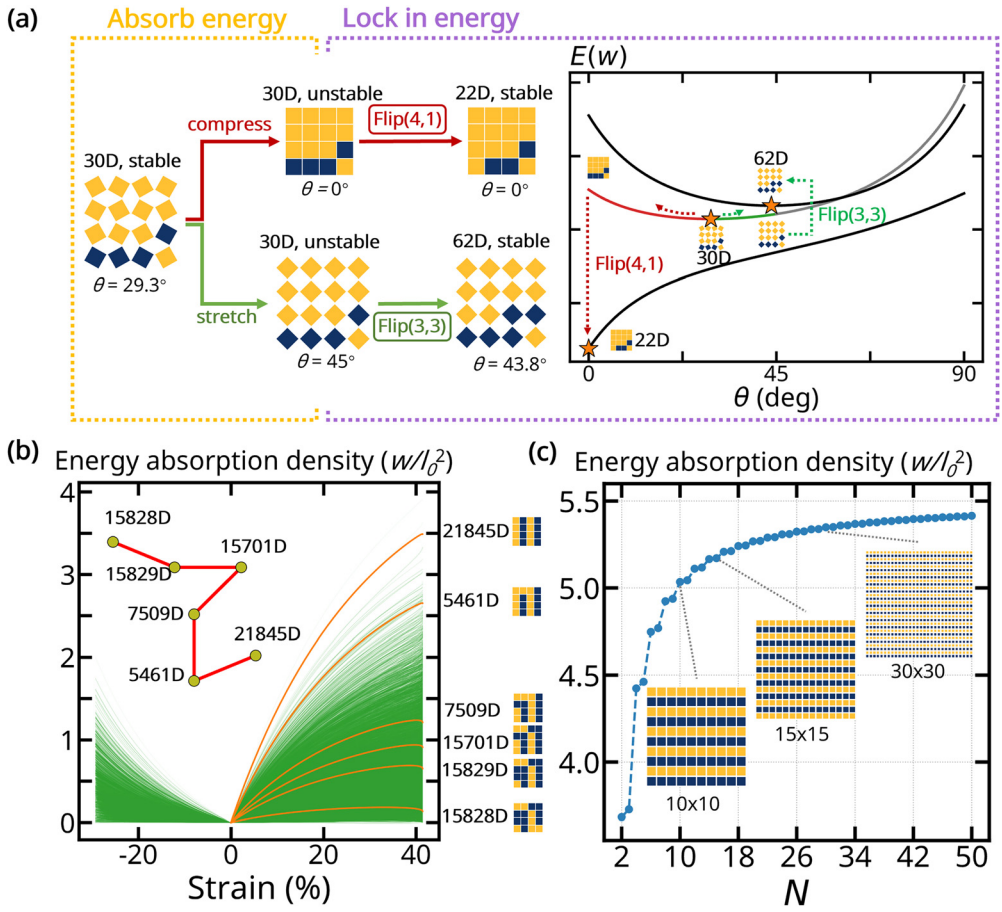

FIG. 4. Digitally reprogrammable energy absorption. (a) Two-stage absorption-locking mechanism illustrated for configuration 30D. Left: Energy capture via deformation along compressive ($\theta \to 0°$) or tensile ($\theta \to 45°$) branches, elevating $E(\theta)$ into a high-energy unstable state. Right: Single-pixel (one-bit) flips transfer the system to a nearby locally stable configuration, thereby locking the stored magnetic energy; coordinated flips can directly reach a global minimum. Energy-angle curves along the entire absorption and locking sequence are shown. (b) Energy absorption density–strain for all 4×4 configurations (green). The highlighted orange curves show a single magnet reconfiguration path that continuously tunes absorption capacity; inset shows the corresponding one-bit trajectory in configuration space. (c) Maximum attainable energy absorption density as a function of system size N, showing rapid growth at small N and saturation at large N.

addressable magnetic pixels. By encoding in-plane magnetic orientations as binary bits and mapping the $2^{N\times N}$ configurations onto an N^2-dimensional hypercube, we enable a systematic exploration of the design space. Combined with Monte Carlo sampling, this framework predicts and classifies energy landscapes into four stability classes and reveals their connectivity via single-bit reconfiguration paths.

Within this predictive framework, we demonstrate that strategic patterning and planned bit-flips enable programmable stiffness and adaptive, multi-stage energy absorption. The digital encoding and hypercube representation together form a discrete, connected graph, which naturally supports algorithmic search and inverse design for target stability, stiffness, and energy dissipation profiles. Beyond the current magnetic system, this framework offers a general tool for material properties and functions, applicable to a wider range of programmable material systems, such as shape memory alloys[44] and metacomposites exhibiting negative permittivity.[45,46] The platform thus suggests promising applications in areas such as modular robotics and impact mitigation. Future extensions could include multi-level magnetization to enrich the response set while preserving digital reconfigurability. It is important to note that the predictive capability of the framework is bounded by the core assumptions of the dipole model. Despite providing specific, experimentally feasible material parameters, the intrinsic simplifications of the model itself inevitably introduce numerical instabilities.[36] And the analysis is based on quasi-static process. To account for more complex factors—such as arbitrary magnet shapes, matrix compliance, and dynamic effects—future work could integrate finite element analysis with machine learning for higher-fidelity modeling and design.[34–37]

See the supplementary material for further details on derivation of the formula, more examples, and other supplementary information related to the main text.

This work is supported by the National Key Technologies R&D Program of China (2022YFA1404700, 2022YFA1207000, and 2021YFA0715302), the National Natural Science Foundation of

China (52101214, 62375054, and 52473254), the Shanghai Rising-Star Program (24QA2700700), the Science and Technology Commission of Shanghai Municipality (24520750200 and 24CL2900200), and the Shanghai Talent Programs. The computations in this research were performed using the Computing for the Future at Fudan (CFFF) platform of Fudan University.

AUTHOR DECLARATIONS

Conflict of Interest

The authors have no conflicts to disclose.

Author Contributions

Qinlian Kang: Data curation (lead); Formal analysis (lead); Investigation (lead); Methodology (lead); Visualization (equal); Writing – original draft (lead); Writing – review & editing (equal). **Jinbo Yang:** Data curation (equal); Formal analysis (equal); Methodology (equal); Software (lead); Visualization (equal); Writing – review & editing (equal). **Chenyang Ji:** Conceptualization (supporting); Methodology (supporting). **Zhijun Lin:** Methodology (supporting). **Songyu Xiong:** Conceptualization (supporting). **Yongfeng Mei:** Supervision (supporting). **Jizhai Cui:** Conceptualization (equal); Funding acquisition (lead); Project administration (lead); Resources (lead); Supervision (lead); Validation (lead); Visualization (equal); Writing – review & editing (lead).

DATA AVAILABILITY

The data that support the findings of this study are available from the corresponding author upon reasonable request.

REFERENCES

[1]P. Jiao, J. Mueller, J. R. Raney, X. Zheng, and A. H. Alavi, "Mechanical metamaterials and beyond," Nat. Commun. **14**, 6004 (2023).
[2]X. Yu, J. Zhou, H. Liang, Z. Jiang, and L. Wu, "Mechanical metamaterials associated with stiffness, rigidity and compressibility: A brief review," Prog. Mater. Sci. **94**, 114 (2018).
[3]X. Zheng, X. Zhang, T.-T. Chen, and I. Watanabe, "Deep learning in mechanical metamaterials: From prediction and generation to inverse design," Adv. Mater. **35**, 2302530 (2023).
[4]Y. Lei, Y. Wang, R. Cui, X. Huang, L. Zhang, Y. Jin, J. Gao, and B. Deng, "3D hyperbolic kirigami metamaterials with tunable auxeticity and multistability," Adv. Sci. **12**, e06703 (2025).
[5]O. Skarsetz, V. Slesarenko, and A. Walther, "Programmable auxeticity in hydrogel metamaterials via shape-morphing unit cells," Adv. Sci. **9**, 2201867 (2022).
[6]T. A. M. Hewage, K. L. Alderson, A. Alderson, and F. Scarpa, "Double-negative mechanical metamaterials displaying simultaneous negative stiffness and negative poisson's ratio properties," Adv. Mater. **28**, 10323 (2016).
[7]Y. C. Wang and R. S. Lakes, "Extreme thermal expansion, piezoelectricity, and other coupled field properties in composites with a negative stiffness phase," J. Appl. Phys. **90**, 6458 (2001).
[8]T. Frenzel, C. Findeisen, M. Kadic, P. Gumbsch, and M. Wegener, "Tailored buckling microlattices as reusable light-weight shock absorbers," Adv. Mater. **28**, 5865 (2016).
[9]C. Coulais, E. Teomy, K. De Reus, Y. Shokef, and M. Van Hecke, "Combinatorial design of textured mechanical metamaterials," Nature **535**, 529 (2016).
[10]R. Guseinov, C. McMahan, J. Pérez, C. Daraio, and B. Bickel, "Programming temporal morphing of self-actuated shells," Nat. Commun. **11**, 237 (2020).
[11]W. Liu, H. Jiang, and Y. Chen, "3D programmable metamaterials based on reconfigurable mechanism modules," Adv. Funct. Mater. **32**, 2109865 (2022).
[12]Y. Zhu, M. Birla, K. R. Oldham, and E. T. Filipov, "Elastically and plastically foldable electrothermal micro-origami for controllable and rapid shape morphing," Adv. Funct. Mater. **30**, 2003741 (2020).
[13]H. Zhang, X. Guo, J. Wu, D. Fang, and Y. Zhang, "Soft mechanical metamaterials with unusual swelling behavior and tunable stress-strain curves," Sci. Adv. **4**, eaar8535 (2018).
[14]A. S. Gliozzi, M. Miniaci, A. Chiappone, A. Bergamini, B. Morin, and E. Descrovi, "Tunable photo-responsive elastic metamaterials," Nat. Commun. **11**, 2576 (2020).
[15]X. Xin, L. Liu, Y. Liu, and J. Leng, "4D pixel mechanical metamaterials with programmable and reconfigurable properties," Adv. Funct. Mater. **32**, 2107795 (2022).
[16]J. K. Choe, J. Yi, H. Jang, H. Won, S. Lee, H. Lee, Y. Jang, H. Song, and J. Kim, "Digital mechanical metamaterial: Encoding mechanical information with graphical stiffness pattern for adaptive soft machines," Adv. Mater. **36**, 2304302 (2024).
[17]Z. Wang, "Digital mechanical metasurfaces for reprogrammable structural display," ACS Nano **17**, 10078 (2023).
[18]F. Pan, Y. Li, Z. Li, J. Yang, B. Liu, and Y. Chen, "3D pixel mechanical metamaterials," Adv. Mater. **31**, 1900548 (2019).
[19]T. Chen, M. Pauly, and P. M. Reis, "A reprogrammable mechanical metamaterial with stable memory," Nature **589**, 386 (2021).
[20]X. Lin, F. Pan, K. Yang, J. Guan, B. Ding, Y. Liu, K. Yang, B. Liu, and Y. Chen, "A stair-building strategy for tailoring mechanical behavior of re-customizable metamaterials," Adv. Funct. Mater. **31**, 2101808 (2021).
[21]W. Lin, Y. Yan, S. Zhao, H. Qin, and Y. Liu, "Digital mechanical metamaterial with programmable functionality," Adv. Mater. **36**, 2406263 (2024).
[22]Z. Meng, H. Yan, M. Liu, W. Qin, G. M. Genin, and C. Q. Chen, "Encoding and storage of information in mechanical metamaterials," Adv. Sci. **10**, 2301581 (2023).
[23]Y. Wei, F. Pan, X. Lin, L. Zhang, J. Xiang, and Y. Chen, "On-demand reprogrammable mechanical metamaterial driven by structure performance relations," Adv. Mater. **37**, 2410865 (2025).
[24]J. D. Jackson, *Classical Electrodynamics*, 3rd ed. (Wiley, New York, 1998).
[25]H. Yasuda, H. Shu, W. Jiao, V. Tournat, and J. R. Raney, "Nucleation of transition waves via collisions of elastic vector solitons," Appl. Phys. Lett. **123**, 051701 (2023).
[26]W. Jiao, H. Shu, V. Tournat, H. Yasuda, and J. R. Raney, "Phase transitions in 2D multistable mechanical metamaterials via collisions of soliton-like pulses," Nat. Commun. **15**, 333 (2024).
[27]H. Yasuda, L. M. Korpas, and J. R. Raney, "Transition waves and formation of domain walls in multistable mechanical metamaterials," Phys. Rev. Appl. **13**, 054067 (2020).
[28]X. Liang, H. Fu, and A. J. Crosby, "Phase-transforming metamaterial with magnetic interactions," Proc. Natl. Acad. Sci. U. S. A. **119**, e2118161119 (2022).
[29]B. Silva, J. Govan, J. Cristóbal Zagal, B. Grossi, A. Roldan, A. S. Nunez, D. Acuña, and H. Palza, "A biomimetic smart kirigami soft metamaterial with multimodal remote locomotion mechanisms," Mater. Des. **233**, 112262 (2023).
[30]Z. Che, X. Wan, J. Xu, C. Duan, T. Zheng, and J. Chen, "Speaking without vocal folds using a machine-learning-assisted wearable sensing-actuation system," Nat. Commun. **15**, 1873 (2024).
[31]W. Jiao, H. Shu, Q. He, and J. R. Raney, "Toward mechanical proprioception in autonomously reconfigurable kirigami-inspired mechanical systems," Philos. Trans. R. Soc., A **382**, 20240116 (2024).
[32]C. Perez-Garcia, R. Zaera, J. Aranda-Ruiz, G. Bordiga, G. Risso, M. L. Lopez-Donaire, K. Bertoldi, and D. Garcia-Gonzalez, "Reprogrammable mechanical metamaterials via passive and active magnetic interactions," Adv. Mater. **37**, e2412353 (n.d).
[33]V. Slesarenko, "Planar mechanical metamaterials with embedded permanent magnets," Materials **13**, 1313 (2020).
[34]C. Perez-Garcia, R. Ortigosa, J. Martínez-Frutos, and D. Garcia-Gonzalez, "Topology and material optimization in ultra-soft magneto-active structures: Making advantage of residual anisotropies," Adv. Mater. e18489 (2025).
[35]X. Gao, M. Yang, A. Pereira, S. Guo, and H. Zhang, "Simulation calculation of selective reflective films based on metamaterials and prediction of color in light filter with machine learning," Eng. Sci. **30**, 1158 (2024).

[36]M. A. Moreno-Mateos, K. Danas, and D. Garcia-Gonzalez, "Influence of magnetic boundary conditions on the quantitative modelling of magnetorheological elastomers," Mech. Mater. **184**, 104742 (2023).
[37]E. M. Stewart and L. Anand, "Magnetostriction of soft-magnetorheological elastomers," J. Mech. Phys. Solids **194**, 105934 (2025).
[38]D. J. Griffiths, *Introduction to Electrodynamics*, 4th ed. (Cambridge University Press, Cambridge, 2017).
[39]L. Lu, S. Leanza, and R. R. Zhao, "Origami with rotational symmetry: A review on their mechanics and design," Appl. Mech. Rev **75**, 050801 (2023).
[40]S. Kamrava, R. Ghosh, Z. Wang, and A. Vaziri, "Origami-inspired cellular metamaterial with anisotropic multi-stability," Adv. Eng. Mater. **21**, 1800895 (2019).
[41]A. Farhan, P. M. Derlet, A. Kleibert, A. Balan, R. V. Chopdekar, M. Wyss, L. Anghinolfi, F. Nolting, and L. J. Heyderman, "Exploring hyper-cubic energy landscapes in thermally active finite artificial spin-ice systems," Nat. Phys. **9**, 375 (2013).
[42]C. El Helou, P. R. Buskohl, C. E. Tabor, and R. L. Harne, "Digital logic gates in soft, conductive mechanical metamaterials," Nat. Commun. **12**, 1633 (2021).
[43]W. Haipeng, L. Shaomin, Z. Qijie, P. Haichun, L. Xiaolin, S. Zhenyu, and S. Peng, "A review of recent research on bionic structural characteristics and performance mechanisms of biomimetic materials," Composites, Part B **304**, 112681 (2025).
[44]Z. Riaz and K. A. Khan, "Next-generation programmable materials: Multifunctionality, smart integration, and industrial frontiers," ES Mater. Manuf. **29**, 1755 (2025).
[45]Z. Wei *et al.*, "Metallic state and negative permittivity in $LaCo_{1-x}Ni_xO_3$ ceramics," Eng. Sci. **21**, 806 (2023).
[46]X. Tang *et al.*, "Flexible carbon nanotubes/polystyrene membranous composites toward ultraweakly and frequency-stable negative permittivity at kHz region," Eng. Sci. **24**, 920 (2023).